NASA/TM–20250011658

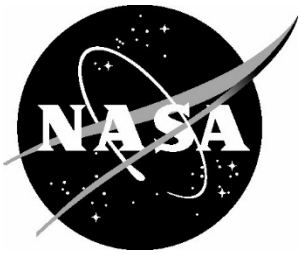

Parameterization of satellite drag acceleration without the use of a global thermosphere model

Daniel, J. Gershman
NASA Goddard Space Flight Center, Greenbelt, MD

January 2026

NASA STI Program Report Series

Since its founding, NASA has been dedicated to the advancement of aeronautics and space science. The NASA scientific and technical information (STI) program plays a key part in helping NASA maintain this important role.

The NASA STI program operates under the auspices of the Agency Chief Information Officer. It collects, organizes, provides for archiving, and disseminates NASA's STI. The NASA STI program provides access to the NTRS Registered and its public interface, the NASA Technical Reports Server, thus providing one of the largest collections of aeronautical and space science STI in the world. Results are published in both non-NASA channels and by NASA in the NASA STI Report Series, which includes the following report types:

- TECHNICAL PUBLICATION. Reports of completed research or a major significant phase of research that present the results of NASA Programs and include extensive data or theoretical analysis. Includes compilations of significant scientific and technical data and information deemed to be of continuing reference value. NASA counterpart of peer-reviewed formal professional papers but has less stringent limitations on manuscript length and extent of graphic presentations.

- TECHNICAL MEMORANDUM. Scientific and technical findings that are preliminary or of specialized interest, e.g., quick release reports, working papers, and bibliographies that contain minimal annotation. Does not contain extensive analysis.

- CONTRACTOR REPORT. Scientific and technical findings by NASA-sponsored contractors and grantees.

- CONFERENCE PUBLICATION. Collected papers from scientific and technical conferences, symposia, seminars, or other meetings sponsored or co-sponsored by NASA.

- SPECIAL PUBLICATION. Scientific, technical, or historical information from NASA programs, projects, and missions, often concerned with subjects having substantial public interest.

- TECHNICAL TRANSLATION. English-language translations of foreign scientific and technical material pertinent to NASA's mission.

Specialized services also include organizing and publishing research results, distributing specialized research announcements and feeds, providing information desk and personal search support, and enabling data exchange services.

For more information about the NASA STI program, see the following:

- Access the NASA STI program home page at http://www.sti.nasa.gov

.

NASA/TM–20250011658

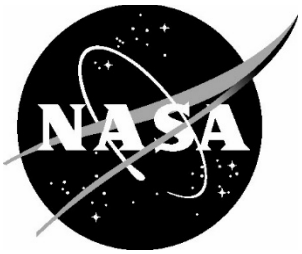

Parameterization of satellite drag acceleration without the use of a global thermosphere model

Daniel, J. Gershman
NASA Goddard Space Flight Center, Greenbelt, MD

National Aeronautics and
Space Administration

NASA Goddard Space Flight Center
Greenbelt, MD

January 2026

The use of trademarks or names of manufacturers in this report is for accurate reporting and does not constitute an official endorsement, either expressed or implied, of such products or manufacturers by the National Aeronautics and Space Administration.

Available from:

NASA STI Program / Mail Stop 050
NASA Langley Research Center
Hampton, VA 23681-2199

Abstract. We introduce a thermosphere-model-agnostic parameterization of time-averaged conditions sampled by satellites in stable Low Earth Orbit (LEO). This method models the total thermospheric mass density or satellite drag acceleration at a given altitude as a linear combination of solar and geomagnetic energy input observables. Using satellite data we demonstrate that this approach results in the successful parameterization over altitudes from ~250 to ~500 km with better than ~15% accuracy. Extrapolation of fit coefficients can maintain this accuracy in support of 7-day forecasts, enabling both improved drag predictions and a more straightforward quantification of uncertainties when provided with predicted energy inputs. This technique can be applied independently for each spacecraft in a constellation without the need for a global thermosphere estimator.

Motivation

Knowledge of the neutral mass density is critical for accurate prediction of satellites, in particular in Low Earth Orbit (LEO) where atmospheric drag can generate significant perturbations of spacecraft trajectories (see *Bruinsma et al.* [2023] and references therein). Models of the thermosphere are typically developed from the lens of scientific research, and aim to provide comprehensive estimates of the entire upper atmosphere [*Jacchia,* 1971; *Picone et al.,* 2002; *Bowman et al.,* 2006,2008; *Emmert et al.,* 2021]. Empirical data drive these models and they are often formulated using 81-day time-centered averages, which implicitly require historical data to maintain accuracy, limiting their use for prediction [*Picone et al.,* 2002; *Bowman et al.,* 2008]. Physics-based models (e.g., *Ridley et al.* [2006]) can be used for prediction, but require significant resources and detailed inputs in order to generate accurate results [*Meng et al.* 2020; *Zhu et al.* 2022]. Here we present a concept for parameterizing variations in neutral mass density observed by a satellite in LEO into its solar and geomagnetic sources. This method generates factors that can then be combined with predicted source terms to estimate future variations in the thermospheric state. Uncertainties in predictions of energy inputs can then be directly converted into uncertainties in neutral mass density. We focus here on orbit-averaged and daily-averaged variations. While there are significant changes in thermospheric mass density with latitude and longitude, accurate quantification of time-averaged variations for LEO satellites captures the net impact of drag on satellite trajectories on operationally relevant timescales.

Approach

Consider a satellite with known ephemeris and a known drag coefficient. Either Two-Line-Element (TLE) tracking [*Picone et al.,* 2005] or GNSS position and velocity data [*Kuang et al.* 2014] can be used to infer the thermospheric mass density. It is not unreasonable to obtain accurate estimates within 24 hours, such that a ‘now-cast’ of the average state of the thermosphere along an orbit is readily achieveable. As a reference, here we leverage total neutral mass density data inferred from the GRACE-CHAMP-GOCE satellites corresponding to an altitude range of ~250 to ~500 km between 2000 and 2024 [*Mehta et al.* 2017; *March et al.,* 2019].

Thermosphere models commonly generate altitude profiles of neutral mass density using an exospheric temperature, i.e, the temperature at the top of the atmosphere. A larger temperature

leads to larger scale heights for atmospheric species and therefore higher mass density at higher altitudes. The Jacchia-Bowman (JB) models [Bowman et al., 2006,2008] utilize two types of energy input: (1) solar UV, which tends to set the baseline level and varies at scales on the order of a solar rotation (i.e., 27 days) or longer, and (2) geomagnetic variations that cause variations on much smaller time scales. For the JB2008 model, solar UV inputs are scaled and combined from a variety of sources such as F10.7, SOHO/SEM, NOAA/SBUV, and GOES/XRS. The model then uses scalings of the Dst geomagnetic index to describe variations in exospheric temperature, though these factors depend on the size of the storm. Derived exospheric temperatures are scaled by correction factors such as day of year and solar activity to form a global thermosphere model.

For operational purposes, there is a critical need to understand the current and near term satellite drag resulting from changes in the thermosphere. On shorter time scales and with operations at a near constant altitude, the complexities associated with seasonal and activity-based corrections are not needed. For a time period in the past defined by τ, the time-averaged (denoted by '<>', here taken as either the orbit average or daily average) exospheric temperature can be approximated simply as,

$$\langle T_{exo} \rangle \approx aS + bG + c \quad (1),$$

where S corresponds to the solar UV input energy, G corresponds to the geomagnetic input energy, and a, b, and c are constants. For a spacecraft that does not significantly change altitude (z) over the course of τ, we approximate that there is a near-linear relationship between $\langle T_{exo} \rangle$ and $\langle \rho(z) \rangle$, such that,

$$\langle T_{exo} \rangle \approx d(z)\langle \rho(z) \rangle + e(z) \quad (2),$$

where d and e are functions of altitude, and therefore constant for a given satellite that is not significantly decaying over time τ. Therefore, we can monitor variations in time-averaged total thermospheric mass density (ρ) sampled by a given satellite as,

$$\langle \rho \rangle \approx fS + gG + h \quad (3),$$

where f, g, and h are constants that are related to the a-e constants in equations (1) and (2). Application of equation (3) does not require direct knowledge of how exospheric temperature relates to mass density at different altitudes and is therefore thermosphere-model-agnostic.

When applying a global thermosphere model, the uncertainty in ρ can be challenging to determine due to the complex and highly non-linear relationship between the inputs and outputs. Fortunately, here uncertainties in $\langle \rho \rangle$ can be readily estimated from uncertainties in S and G (defined as σ_S and σ_G, respectively), i.e.,

$$\sigma_{\langle \rho \rangle} \approx \sqrt{f^2\sigma_S^2 + g^2\sigma_G^2} \quad (4).$$

One could alternatively solve directly for variations in $\langle a_{drag} \rangle$ for a given satellite, which is the time-averaged acceleration due to thermospheric drag, calculated as,

$$\langle a_{drag} \rangle \approx \langle \frac{1}{2} \rho B v_{sc}^2 \rangle \quad (5),$$

where v_{sc} is the spacecraft orbital speed and B is the inverse satellite ballistic coefficient [*Picone et al.* 2005]. We assume v_{sc} is well known from satellite tracking data. Here, B does not need to be solved for directly, but does need to be either stable over time τ. Parameterizing drag acceleration results in a similar form to equations (1) and (3) but with different constant coefficients (α, β, γ), i.e.,

$$\langle a_{drag} \rangle \approx \alpha S + \beta G + \gamma \quad (6).$$

As will be discussed, an additional scaling factor may need to be included in equation (6) to account for relative variations in B inferred from tracking and operations data. Such effects are not considered here. Significant variations of B over time interval τ would likely result in equation (3) being more applicable for implementation.

Similar to equation (4), we can quantify the uncertainty in $<a_{drag}>$ in terms of the uncertainties of S and G as,

$$\sigma_{\langle a \rangle} \approx \sqrt{\alpha^2 \sigma_S^2 + \beta^2 \sigma_G^2} \quad (7).$$

A summary of the proposed approach for predicting satellite drag compared to the traditional method is shown in Figure 1. Traditionally, the date, satellite position, and solar and geomagnetic activity indices (S and G, respectively) are input into a global thermosphere model to estimate total neutral mass density (ρ) and composition at a given location. Predictions of inputs whether through extrapolation, orbit propagation, or other methods, would be needed to generate estimates of ρ in the future. An estimate of the coefficient B over that time period (which may include thermospheric composition effects) as well as the satellite velocity would be used to generate an estimate of a_{drag}, which describes the satellite drag acceleration. Uncertainties of a_{drag} are not necessarily straightforward to generate since there are uncertainties in the prediction of both satellite positions and energy sources, as well as a highly non-linear relationship between model inputs and outputs. Alternatively, using past measurements of time-averaged $<a_{drag}>$ or $<\rho>$, S, and G from time (t-τ) to time t, we generate model fit parameters (α, β, γ) or (f, g, h). These parameters are used to scale predictions of S and G to generate estimates of $<a_{drag}>$ or $<\rho>$ and their uncertainties for current and future times. No forward-propagated satellite positions, nor absolute knowledge of the satellite drag coefficient B, are required, though relative changes in B may be needed to be incorporated if variations are significant over time τ.

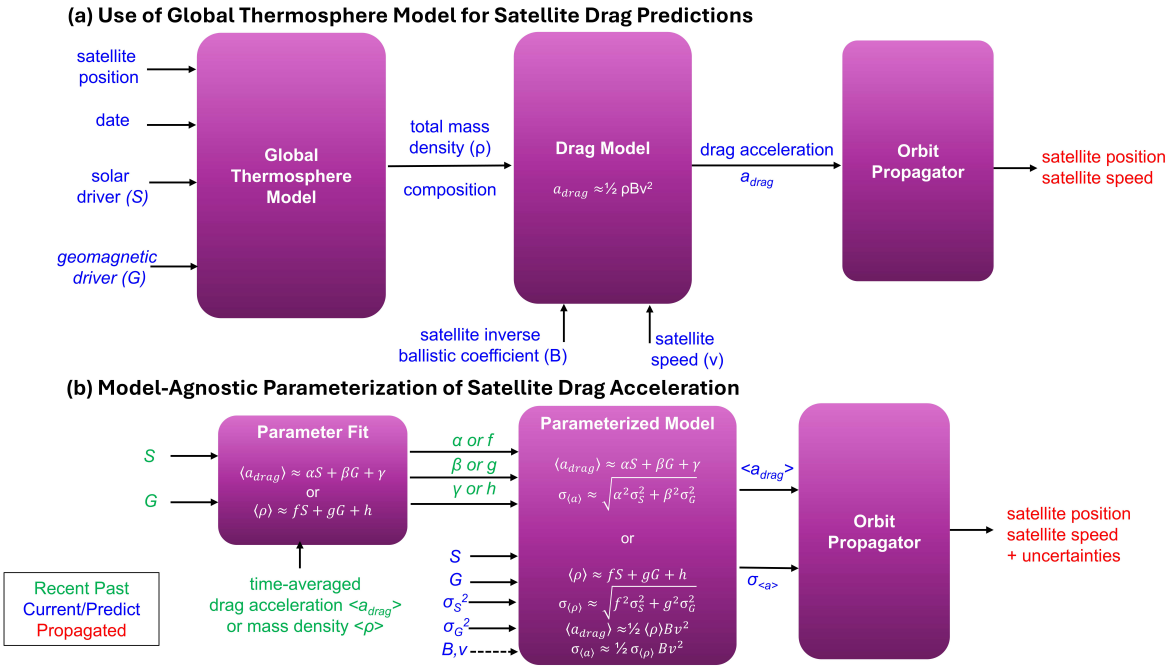

Figure 1. (a) Traditional approach to estimating satellite drag utilizing a global thermospheric model (adapted from *Bruinsma et al.* [2023]) for the case of a stable satellite *B*-factor not strongly driven by composition). (b) Alternative approach presented in this work that parameterizes past observations of drag acceleration or thermospheric mass density and energy source terms to generate predictions with readily quantified uncertainties.

Proof of Concept

A variety of sources can be used as *S* and *G* inputs. Here for *S* we use the daily-averaged E10.7 index derived from TIMED/SEE data, which corresponds to the integrated EUV irradiance between 1 and 105nm. We low pass filter the solar energy input data with an RC time constant of 48 hours to smooth data and incorporate a time lag between solar UV energy input and global thermospheric heating. This time constant was coarsely optimized to maximize fit accuracy for the example below. Other solar observables or indices (e.g., F10.7 index, SOHO/SEM, NOAA/SBUV, GOES/XRS) should also be suitable for use. The best performance is anticipated for observables associated with measuring solar UV flux, as these photons directly heat the thermosphere and generate increases in mass density at higher altitudes [*Bowman et al.,* 2008].

The JB2008 model uses Dst as its equivalent of *G* as it is well correlated with enhancement in neutral density [*Bowman et al.,* 2008]. However, there are several other options that may result in improved performance, in particular for predictions. For example, *Weimer et al.* [2011] describes a replacement for the *G* term in JB2008 that utilizes interplanetary magnetic field and solar wind data. In addition, as shown in Figure 2, total field-aligned current (FAC) or total precipitating electron current can also serve as inputs for *G* because they correlate well with short term density enhancements. Here the total FAC is provided by AMPERE, which fits perturbations of magnetometer data from the Iridium satellites at 780 km from a reference IGRF magnetic field model with spherical harmonics to estimate global and spatially-resolved field-aligned current densities [*Anderson et al.* 2000]. The AMPERE-approach should be feasible to implement for other LEO constellation with magnetometers (e.g., *Parham et al.* [2019]), and likely with lower latency than the public release of AMPERE data products. Precipitating

electron current can be calculated from the SSJ instrument on the DMSP satellites using their auroral precipitation data product (*Redmon et al.,* 2017). Here, we calculate orbit-averaged latitudinal averages of electron flux from the F16, F17, and F18 active DMSP satellites. We then integrate over each hemisphere to estimate the total precipitating electron current. This electron current, as shown in Figure 2 is well correlated with the total AMPERE-derived FACs. Current enhancements precede an increase in thermospheric mass density by several hours during major storms providing a predictive capability during times when the drag hazard is at its highest

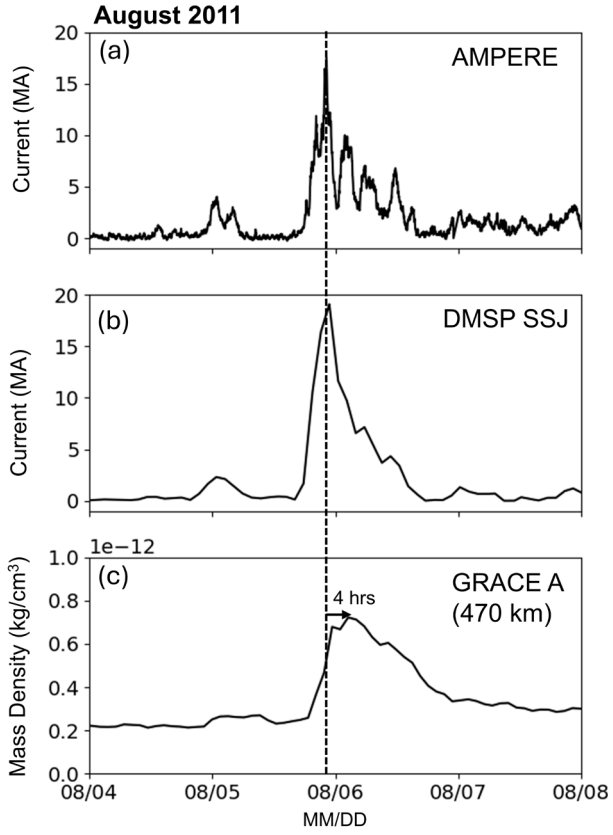

Figure 2. (a) AMPERE-derived total FAC, (b) DMSP/SSJ-derived total electron current, and (c) GRACE-derived total thermospheric mass density at 470 km for a geomagnetic storm in August 2011. Both currents correlate well with variations in mass density and large currents precede major enhancements in density by several hours.

For an initial demonstration, we choose to use the total FAC inferred from AMPERE to represent *G*. To precondition the FAC data, we average together the AMPERE-provided upward total currents in the northern and southern hemispheres, time-average to match the mass density time series cadence, subtract off a quiet-time offset determined to be ~0.5MA, and perform low-pass filtering with a RC time constant of 18 hours to smooth data and account for a lag between energy input and increases in thermospheric density. This time constant was coarsely optimized to maximize fit accuracy for the example below. Geomagnetic indices (e.g., Dst, AE, Ap), global-averaged electron precipitation (e.g., DMSP/SSJ), or the *Weimer et al.* [2011] model also should be suitable for use. Finally, we will use estimates of <ρ> from the GOCE-CHAMP-GRACE satellites [*Mehta et al.* 2017; *March et al.,* 2019].

For each data point t, we generate historical time series between time t-τ and time t of <*ρ*>, *S*, and *G*, where τ = 27 days for this example. We then perform a least-squares fit using equation (3) to solve for coefficients *f*, *g*, and *h* that will be used to parameterize the total neutral mass

density at time *t*. Because the *G* time series has a small residual offset (due to quiet-time offset removal described in the previous paragraph), it does not generate a strong contribution to *h*. We can therefore approximate the solar and geomagnetic contributions to variations in mass density as 'fS+h' and 'gG' respectively. This parameterization is illustrated in Figure 3 for two intervals (4/1/2010-7/1/2010 and 4/1/2024-7/1/2024). This simple fit successfully captures the variability in the orbit-averaged thermospheric mass density. We use the root-mean-square percentage error as a goodness-of-fit metric, defined as,

$$\mathrm{RMSPE} = 100\% \cdot \sqrt{\frac{\sum_{i=1}^{n}\left(1-\frac{\langle\rho\rangle_f}{\langle\rho\rangle_m}\right)^2}{n}} \qquad (8),$$

where n is the number of data points in time τ and $\langle\rho\rangle_f$ and $\langle\rho\rangle_m$ are the fit and measured values of $\langle\rho\rangle$, respectively. These results demonstrate the suitability of simple solar UV and geomagnetic activity observables for accurately modeling orbit-averaged variations in thermospheric mass density within ~10-15%.

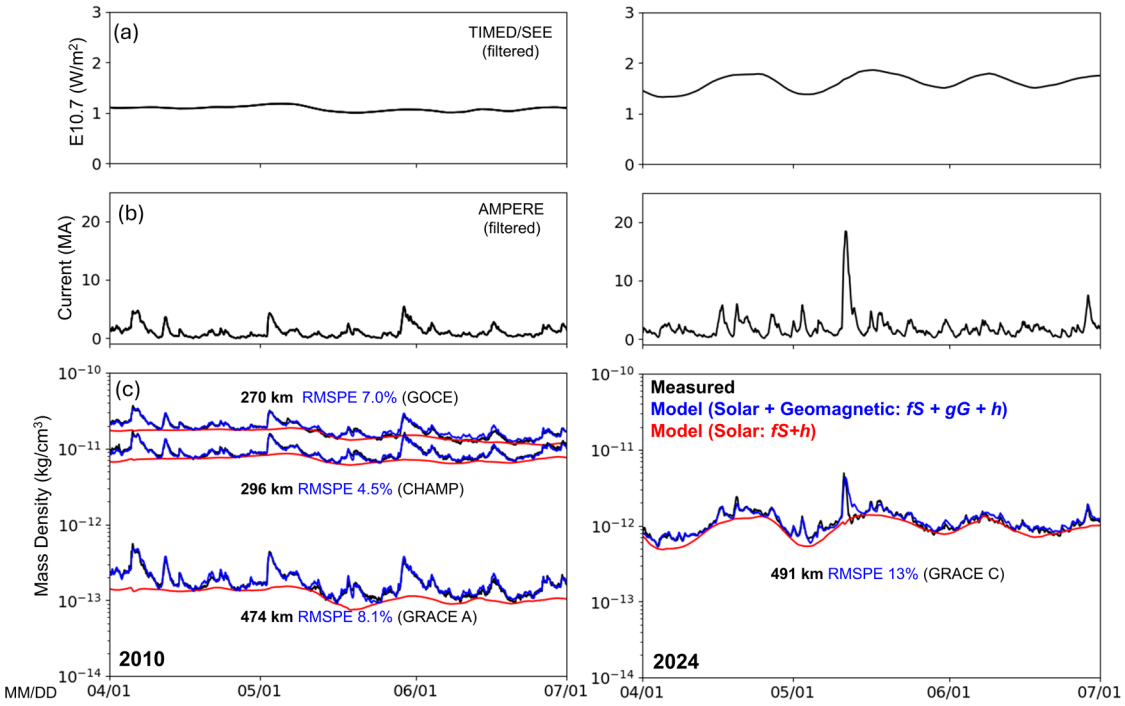

Figure 3. (a) low-pass-filtered E10.7 index (i.e., *S* in equation (3)) from TIMED/SEE integrated EUV irradiance from 1 to 105nm, (b) low-pass-filtered total field-aligned current (i.e., *G* in equation (3)) from AMPERE, (c) thermospheric mass density (i.e., <ρ> in equation (3)) from GOCE, CHAMP, and GRACE for two four month intervals (4/1/2010-7/1/2010 (left) and 4/1/2024-7/1/2024 (right)). The results of the model fit to equation (3) are included using intervals of τ = 27 days. The orbit-averaged variations of neutral mass density (black curve) at different altitudes are well captured by the combination of solar and geomagnetic terms (blue curve), even during extreme geomagnetic storms such as the Gannon storm on May 10-11, 2024 observed by GRACE-FO. Solar-only contributions to the neutral mass density are indicated by the red curves. Root Mean Square Percentage Error (RMSPE) calculated between the blue and black curves are included for each satellite.

To evaluate the effectiveness of the presented technique for scaling predictions of S and G, we repeat the fits used to generate Figure 3 for different sets of time windows. For a given time t, we determine parameters $f,g,$ and h using data between $t - \delta\tau$ and $t+(1-\delta)\tau$. For $\delta = 0$, current and future data is used to determine fit parameters (i.e., times between t and $t+\tau$). For $\delta = 0.5$, the fit is centered on the current time (i.e., times between $t-\tau/2$ and $t+\tau/2$). For $\delta = 1$, which was used to generate Figure 3, past and current data is used (i.e., times between $t-\tau$ and t). Finally, for $\delta>1$, only past data is used. A value of $\delta=1.259$ corresponds to a 7 day prediction interval (i.e., only data from $t-34$ days to $t-7$ days is used to estimate scaling parameters that would be used for time t). RMPSE as a function of δ is shown in Figure 4 for the intervals above using $\tau = 27$ days. The minimum error occurs near center-averaged case of $\delta\approx0.5$. The result remains accurate to within 15% for $\delta < 1.259$ in all cases, demonstrating the viability of utilizing fit parameters derived from past data in support of future predictions

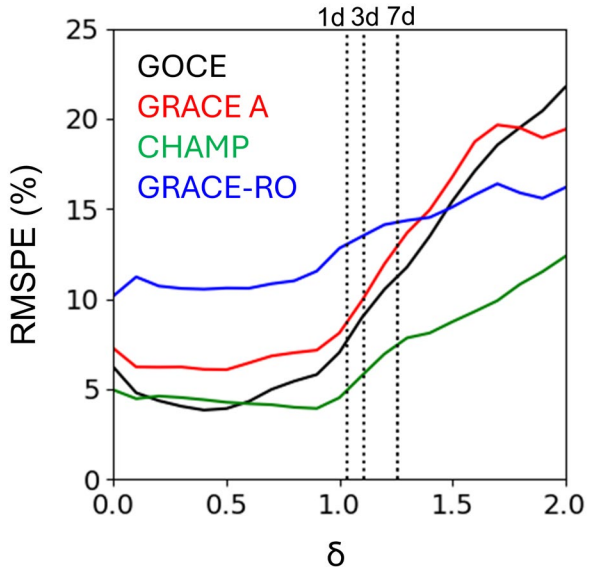

Figure 4. RMSPE as a function of δ for the GOCE-CHAMP-GRACE satellites for the intervals shown in Figure 3. The more accurate parameterization fit occurs near the time-centered case of δ≈0.5. The δ values corresponding to 1-day, 3-day, and 7-day prediction intervals are indicated as vertical dotted lines.

Finally, we present an example application of our technique for the parameterization of $\langle a_{drag} \rangle$ from commercial LEO satellites. Here we use the publicly available daily TLE tracking data from https://ephemerides.planet-labs.com for the 'SKYSAT C10' and 'SKYSAT C14' satellites for 11/1/2023 through 8/1/2024. As shown in Figure 5, we apply the method developed by *Picone et al.* [2005] to derive daily-averaged $\langle a_{drag} \rangle$ for each spacecraft and use E10.7 and AMPERE-based observables to model the energy sources S and G, respectively. We then solve for coefficients α, β, and γ in equation (6) using $\tau = 27$ days and $\delta = 1$ to estimate $\langle a_{drag} \rangle$ at time t. The RMSPE of the model fits are ~10-15% for both satellites over this interval despite having no *a priori* knowledge of spacecraft attitude, maneuvers, or B-factors.

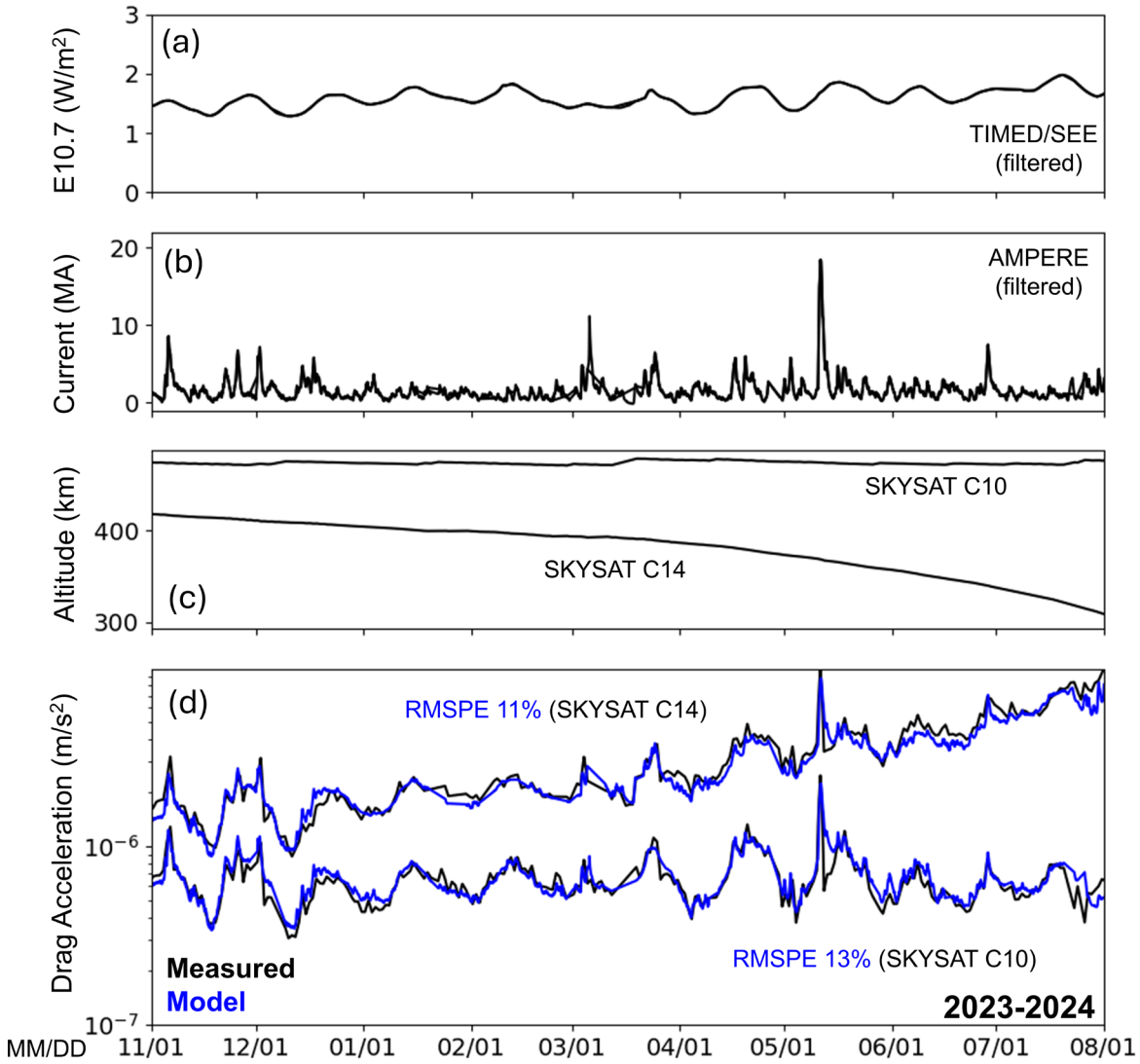

Figure 5. (a) low-pass-filtered E10.7 index (i.e., *S* in equation (3)) from TIMED/SEE integrated EUV irradiance from 1 to 105nm, (b) low-pass-filtered total field-aligned current (i.e., *G* in equation (3)) from AMPERE, and (c) altitude and (d) drag acceleration ($<a_{drag}>$) for two commercial LEO satellites (SKYSAT C10 and SKYSAT C14). The orbit-averaged variations of drag acceleration (black curve) at different altitudes are well captured by the combination of solar and geomagnetic terms (blue curve). Root Mean Square Percentage Error (RMSPE) calculated between the blue and black curves are included for each satellite. No independent of determination of the total thermospheric mass density or the satellite *B*-factor was needed to accurately parameterize variations in $<a_{drag}>$ in terms of solar and geomagnetic drivers.

Discussion

The choice of averaging interval time τ will impact the performance of both the model fit and the extrapolation quality. At low values of τ, the model will overfit the data such that reduced fitting errors are expected, but the ability to extrapolate the coefficients to obtain meaningful results for future data becomes limited. At increasingly larger values of τ, a constant set of model coefficients will not be able to describe the variability, in particular as effects associated with spacecraft altitude changes and seasonal/secular variability in the thermosphere become more

significant. A reasonable choice in τ can also compensate for systematic variations in the observables themselves that occur over time (e.g., degradation in TIMED/SEE over several decades of operations). The examples shown here correspond to $\tau = 27$ days, i.e., a single solar rotation, which was coarsely selected to balance these factors. A more detailed sensitivity study should determine the optimal value of τ for a given implementation. Finally, it may be possible to incorporate additional terms into equations (3) and (6) to compensate for some of these longer-term variabilities, as well as for other effects such as altitude-variability.

Changes in satellite attitude may result in significant changes to its *B*-factor over the course of interval τ. An overall scaling of equation (6) based on estimated relative variations in *B* associated with known attitude changes could compensate for these effects. The advantage of the presented technique here is that even for the case where these relative variations need to be taken into account, absolute and fully independent determinations of *B* and ρ are not required in order to generate future predictions. Thermospheric composition may also contribute to changes in B, which is less straightforward to correct for. However, for short intervals, only during the most extreme storms are such changes likely to systematically bias the parameter fits.

Improved energy source observables will enable improved model fits. Additional pre-conditioning of data may also lead to improved performance for a given observable, in particular optimizing the time lags, averaging, filtering, compensating for the potentially non-linear response of the thermosphere to large energy inputs [*Weimer et al.* 2011] or modeling the intensity-dependent cooling times of the thermosphere to its previous state [*Zesta and Oliveira,* 2019]. Extrapolation quality may be improved through more careful trending of previous model fits or adjustments of τ as discussed. Techniques to provide future predictions of energy source observables are beyond the scope of this initial work. However, we note that if the uncertainty in these predictions can be quantified, it is straightforward to propagate uncertainties in *S* and *G* terms into satellite $<\rho>$ and $<a_{drag}>$ per equations (4) and (7). Our approach therefore provides drastically simplified quantification of uncertainties in predicted thermospheric mass density compared to those generated using global thermosphere models.

Successful application of the presented technique to a constellation of LEO spacecraft could be leveraged to interpolate or extrapolate values of thermospheric mass density to multiple orbit-planes and/or altitudes. These values could be used to constrain a global thermosphere model as appropriate, in particular to aid in the inference of composition at lower altitudes. In addition, fit parameters initial calculated from daily-averages derived from TLE-data can be used to scale hourly *S* and *G* observables. This scaling results in a set of finer resolution, orbit-averaged estimates of satellite drag even in the absence of high-cadence tracking data.

Geomagnetic energy input is localized at high-latitudes, leading to localized heating and enhancements of thermospheric mass density. These enhancements then propagate to lower latitudes, resulting in a globally increased thermospheric temperature within a few hours [*Weimer et al.* 2023]. While the physics of this redistribution process is highly complex and still under active study, the use of orbit-averages here largely mitigates the impact of these spatially localized uncertainties. If quantification of neutral density variations along a satellite orbit is needed, the methodology presented here could be used to constrain or scale a more comprehensive thermosphere model using data assimilation techniques.

Finally, the calculation of FACs from magnetometer data requires ground processing and detrending, limiting its use on-orbit. However, an *in situ* electron sensor could provide an on-board warning for impending increases in satellite drag based on its measured fluxes. Although the two observables can serve as interchangeable sources of *G* for the drag predictions presented here, global maps of field aligned currents and electron precipitation would exhibit significantly different spatial structures and could potentially be combined together to directly solve for the full electrodynamics of the upper atmosphere, including ionospheric conductivity, electric field, convection patterns, and Joule heating [*Weimer et al.* 2005; *Newell et al.,* 2009; *Robinson et al.,* 2021].

Concluding Remarks

We have developed a technique to parameterize and extrapolate orbit-averaged variations in neutral mass density and satellite drag acceleration into its solar and geomagnetic drivers without the need for a global thermosphere model. In the examples provided using both science and commercial satellite data from altitudes ~250km to ~500km, this approach can achieve better than ~15% accuracy averaged over a given satellite orbit. In addition, we demonstrate that this accuracy is maintained for the application of model fit coefficients for t+7 day forecasts. Therefore, prediction uncertainties should be dominated by errors in energy source predictions and can be more readily quantified. The presented approach naturally anchors predictions to 'now-cast' observations, ensuring that systematic biases in altitude, seasonal, and solar activity present in global thermosphere models are mitigated.

Acknowledgements. This work was supported by NASA Heliophysics. We gratefully acknowledge A. Glocer for his review and valuable feedback on this work.

References

Anderson, B. J., Takahashi, K., & Toth, B. A. (2000). Sensing global Birkeland currents with iridium® engineering magnetometer data. *Geophysical Research Letters,* 27(24), 4045–4048. https://doi.org/10.1029/2000gl000094

Bruinsma, S., Dudok de Wit, T., Fuller-Rowell, T., Garcia-Sage, K., Mehta, P., Schiemenz, F., et al. (2023). Thermosphere and satellite drag. *Advances in Space Research*. https://doi.org/10.1016/j.asr.2023.05.011

Bowman, B. R., Kent Tobiska, W., Marcos, F. A., & Valladares, C. (2008). The JB2006 empirical thermospheric density model. *Journal of Atmospheric and Solar-Terrestrial Physics*, 70, 774–793. https://doi.org/10.1016/j.jastp.2007. 10.002

Bowman, B., Tobiska, W. K., Marcos, F., Huang, C., Lin, C., & Burke, W. (2008). A new empirical thermospheric density model JB2008 using new solar and geomagnetic indices. In *AIAA/AAS Astrodynamics Specialist Conference and Exhibit*, Honolulu, Hawaii. https://doi.org/10.2514/6.2008-6438

Emmert, J. T., Drob, D. P., Picone, J. M., Siskind, D. E., Jones, M. Jr., Mlynczak, M. G., et al. (2021). NRLMSIS 2.0: A whole-atmosphere empirical model of temperature and neutral species densities. *Earth and Space Science*, 8, e2020EA001321. https://doi.org/10.1029/2020EA001321

Jacchia, L. G. (1971). Revised static models of the thermosphere and exosphere with empirical temperature profiles. SAO special report 332.

Kuang, D., Desai, S., Sibthorpe, A., & Pi, X. (2014). Measuring atmospheric density using GPS-LEO tracking data. *Advances in Space Research*, **53**(2), 243–256. https://doi.org/10.1016/j.asr.2013.11.022

March, G. E., Doornbos, N., & Visser, P. N. A. M. (2019). High-fidelity geometry models for improving the consistency of CHAMP, GRACE, GOCE and Swarm Thermospheric Density Data Sets. *Advances in Space Research*, **63**(1), 213–238. https://doi.org/10.1016/j.asr.2018.07.009

Mehta, P. M., A. C. Walker, E. K. Sutton, and H. C. Godinez (2017), New density estimates derived using accelerometers on board the CHAMP and GRACE satellites, *Space Weather*, 15, 558–576, doi:10.1002/2016SW001562.

Meng, X., Mannucci, A. J., Verkhoglyadova, O. P., Tsurutani, B. T., Ridley, A. J., & Shim, J.-S. (2020). Thermosphere-ionosphere modeling with forecastable inputs: Case study of the June 2012 high-speed stream geomagnetic storm. *Space Weather*, 18, e2019SW002352. https://doi.org/10.1029/2019SW002352

Newell, P. T., T. Sotirelis, and S. Wing (2009), Diffuse, monoenergetic, and broadband aurora: The global precipitation budget, *J. Geophys. Res.*, 114, A09207, doi:10.1029/2009JA014326.

Parham, J. B., Beukelaers, V., Leung, L., Mason, J., Walsh, B., & Semeter, J. (2019). Leveraging commercial cubesat constellations for auroral science: A case study. *Journal of Geophysical Research: Space Physics*, 124, 3487–3500. https://doi.org/10.1029/2018JA025966

Picone, J. M., A. E. Hedin, D. P. Drob, and A. C. Aikin, (2002), NRLMSISE-00 empirical model of the atmosphere: Statistical comparisons and scientific issues, *J. Geophys. Res.*, 107(A12), 1468, doi:10.1029/2002JA009430.

Picone, J. M., J. T. Emmert, and J. L. Lean (2005), Thermospheric densities derived from spacecraft orbits: Accurate processing of two-line element sets, *J. Geophys. Res.*, 110, A03301, doi:10.1029/2004JA010585.

Redmon, R. J., W. F. Denig, L. M. Kilcommons, and D. J. Knipp (2017), New DMSP database of precipitating auroral electrons and ions, *J. Geophys. Res. Space Physics*, 122, 9056–9067, doi:10.1002/2016JA023339.

Ridley, A. J., Deng, Y., & Tóth, G. (2006). The global ionosphere-thermosphere model. *Journal of Atmospheric and Solar-Terrestrial Physics*, 68, 839–864. https://doi.org/10.1016/j.jastp.2006.01.008

Robinson, R. M., Zanetti, L., Anderson, B., Vines, S., & Gjerloev, J. (2021). Determination of auroral electrodynamic parameters from AMPERE field-aligned current measurements. *Space Weather*, 19, e2020SW002677. https://doi.org/10.1029/2020SW002677

Weimer, D. R. (2005), Improved ionospheric electrodynamic models and application to calculating Joule heating rates, *J. Geophys. Res.*, 110, A05306, doi:10.1029/2004JA010884.

Weimer, D. R., B. R. Bowman, E. K. Sutton, and W. K. Tobiska (2011), Predicting global average thermospheric temperature changes resulting from auroral heating, *J. Geophys. Res.*, 116, A01312, doi:10.1029/2010JA015685.

Weimer, D. R., Mehta, P. M., Licata, R. J., & Tobiska, W. K. (2023). Global variations in the time delays between polar ionospheric heating and the neutral density response. *Space Weather*, 21, e2022SW003410. https://doi.org/10.1029/2022SW003410

Zesta, E., & Oliveira, D. M. (2019). Thermospheric heating and cooling times during geomagnetic storms, including extreme events. *Geophysical Research Letters*, 46, 12739–12746. https://doi.org/10.1029/2019GL085120

Zhu, Q., Deng, Y., Sheng, C., Anderson, P., & Bukowski, A. (2022). Impact of soft electron precipitation on the thermospheric neutral mass density during geomagnetic storms: GITM simulations. *Geophysical Research Letters*, 49, e2021GL097260. https://doi.org/10.1029/2021GL097260